Supplemental Information

Sub-micrometer-precision, three-dimensional (3D) hydrodynamic focusing *via* "microfluidic drifting"

Ahmad Ahsan Nawaz,[a] Xiangjun Zhang,[b] Xiaole Mao,[a,c] Joseph Rufo,[a] Sz-Chin Steven Lin,[a] Feng Guo,[a] Yanhui Zhao,[a] Michael Lapsley,[a] Peng Li,[a] J. Philip McCoy,[d] Stewart J. Levine [d] and Tony Jun Huang[a,c]

[a] Department of Engineering Science and Mechanics, The Pennsylvania State University, University Park, PA 16802, USA.
Fax: 814-865-9974; Tel: 814-863-4209; E-mail: junhuang@psu.edu
[b]State Key Laboratory of Tribology, Tsinghua University, Beijing, 100084, P.R. China
[c] Department of Bioengineering, The Pennsylvania State University, University Park, PA 16802, USA
[d]National Heart, Lung, and Blood Institute at NIH, Bethesda, MD 20892, USA

Theoretical and numerical analysis of particle-focusing process:

As the particles flow inside a "microfluidic drifting" 3D focusing device, they experience a number of forces, including centrifugal force ($F_{cfg} \sim {}^{1}/_{6}(\rho_p - \rho_L)\pi d^3 U_p^2/R$), viscous drag force ($F_D \sim 3\pi\mu U_D d$), gravitational force ($F_G \sim {}^{1}/_{6}(\rho_p - \rho_L)g\pi d^3$), wall effects, buoyant force, and shear forces due to a difference in the velocity of the sample fluid and the vertical sheath fluid. In the above equations, ρ_P and ρ_L are the densities of the particle and the fluid, respectively, d is the diameter of particle, U_F is the velocity of the fluid, U_D is the velocity of the fluid due to Deans vortices, R is the radius of curved channel, g is the acceleration due to gravity, and μ is the viscosity of the fluid. By systematically controlling the channel geometries and the fluid velocities, we were able to precisely balance the forces and significantly improve the focusing precision. Of the above-mentioned forces, F_{cfg} and F_G increase rapidly as the diameter of the particles increase and F_D plays a dominant role for small particles. Inertial effects that cause the particles to migrate across streamlines are less dominant and the micro particles tend to follow streamlines. To study the relative effect of the underlying forces responsible for particle positioning, we use particles with a diameter of 1.9 μm in our following calculations. Assuming $U_P=U_L=0.56$ m/s, $U_D=0.12$ m/s (from CFD simulations), $\rho_P=1.07 \times 10^3$ Kg/m^3, $\rho_L=1 \times 10^3$ Kg/m^3, F_D dominates with ~1.9 nN as compared to F_{cfg} (~ 0.32 pN) and F_G (2.5 fN). Fig. S1(a) summarizes the magnitude of different forces acting on the particles with different diameters. Our results indicate that for the "microfluidic drifting" device with a curvature angle of 180^0, particles/cells ranging from submicron to several tens of microns will follow streamlines. In Fig. S1(b) the spray module of the CFD software has been utilized to visualize the behavior of polystyrene particles as they flow within the 180^0 curved microfluidic channel. The color indicated by the color bar depicts the height at which polystyrene particles are present. The particles are introduced randomly at the sample inlet at different vertical positions. As the particles move around the curve, the centrifugal forces resulting from counter-rotating vortices bring the particles from the inner wall position to the center plane position. As the particles reach the end of the curved path, the green color indicates their vertical focusing. The horizontal sheath fluids pinch the particles into a single file line, keeping them in the same vertical plane, which can be seen in the downstream straight channel. Moreover, the velocity of the midstream is indicated to be 1.4 m/s shown in Fig. S1(c).This flow velocity is lower than that generally required in conventional flow cytometers.[4] Hence, less damage to cells due to shear stress is anticipated.

Characterization of particle focal-diameter:

Videos that characterize the particle-focusing process were acquired at 225,000 frames per second and analyzed with Image-J software. For each channel device, 10 particles were selected approaching the straight downstream channel via the curved channel path at different regions ranging from channel inner wall to channel middle as shown in Fig. S2(a), though the trajectories of only two particles are shown (z-stack of images). The image indicates that the particles remain focused 5 mm downstream (Fig. S2(b)). Via Image J, the pixels were assigned a value for a known distance. At the downstream, deviation of the 10 different polystyrene beads was noted from the channel middle. The average of the deviation was then calculated for standard deviation. With the 180^0 channel design, 1.9 µm polystyrene beads were found to be focused into a focal diameter of 2.8 µm; hence, a standard deviation of ±0.45 µm was achieved in particle position.

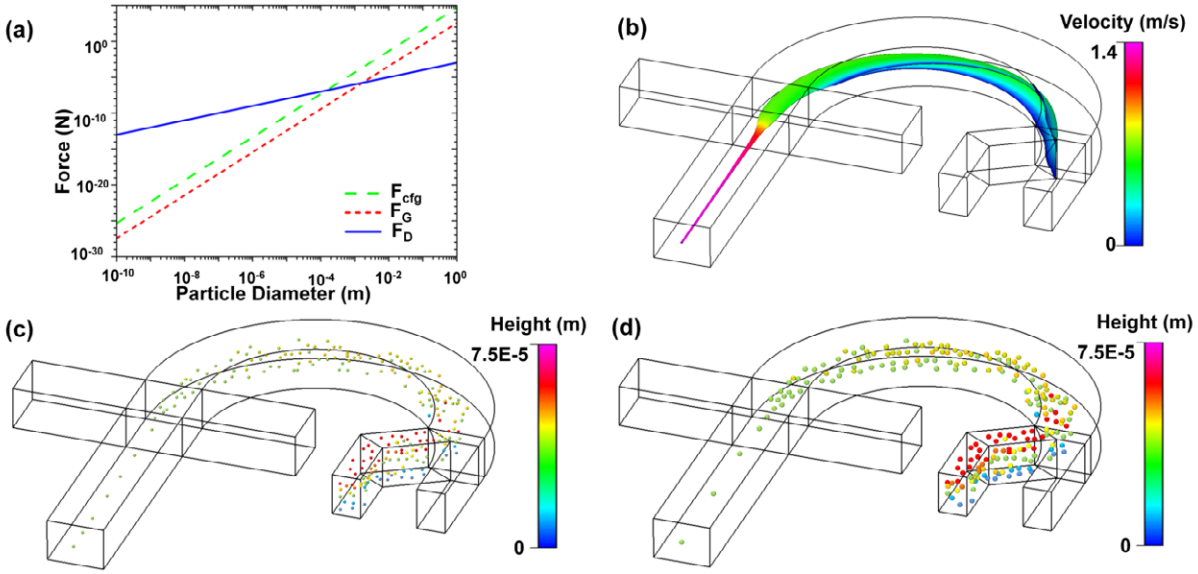

Fig. S1: (a) Relationship between the primary forces acting on a particle and the diameter of the particle. The parameters used were obtained from CFD simulations. When the diameter of the particle is at the micrometer scale (10^{-6} m), the viscous drag force dominates and the particle follows streamlines, resulting in tight particle focusing. (b) CFD simulation results indicate that the midstream velocity of the sample fluid reaches 1.4 m/s as indicated by the pink color from the color bar. (c and d) CFD simulation of polystyrene beads (2 µm and 10 µm) are focused at the mid-plane as they move around the curve and ultimately form a single file line of particles at the downstream while maintaining the height, as indicated by the color of the beads.

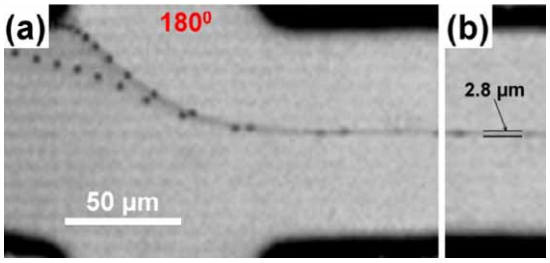

Fig. S2: 1.9 µm polysterene beads are focused via 180^0 channel device.

8-Peak rainbow bead calibration test:

To further characterize the performance of our devices, we subjected the 90^0, 135^0, 180^0, and 225^0 particle-focusing devices to 8-peak rainbow bead calibration test. The improvement in the sensitivity could then be visualized. Spherotech (BD, Biosciences) calibration beads (3−3.4 µm) which exhibit eight populations of different fluorescence intensities were used to evaluate the different focusing devices. Fig. S3 shows the histogram plot of fluorescence intensity results obtained with 90^0, 135^0, 180^0, and 225^0 particle-focusing devices. An obvious improvement in the sensitivity can be observed as the angle is increased from 90^0 to 180^0. With the 90^0 focusing device, the 6^{th}, 7^{th}, and 8^{th} peaks are not resolved as separate peaks. This can be attributed to the swaying of the beads within the 25 µm focusing diameter of the sample stream. Much improvement in results with the 135^0 and 225^0 focusing devices is seen as the focusing diameter reduces to ~ 8.5 µm as compared to the former case; however, the 7^{th} and 8^{th} peak are not well separated. With the 180^0 focusing device (Fig. S3(c)), well distinguished and separated eight peaks can be seen. Moreover, an increase in the detected fluorescent intensity is depicted with the 180^0 focusing device, when compared to the 90^0 and 135^0 devices. The improvement in precision, as well as the decrease in midstream sample flow velocity (3.6 m/s, 2.8 m/s, and 1.4 m/s (Fig. S1(b)) for 90^0, 135^0 and 180^0 focusing devices respectively), can be attributed to this observation. Hence, the microflow cytometry device with a curvature angle of 180^0 indicates the ability to perform high-resolution detection like its commercial counterparts.

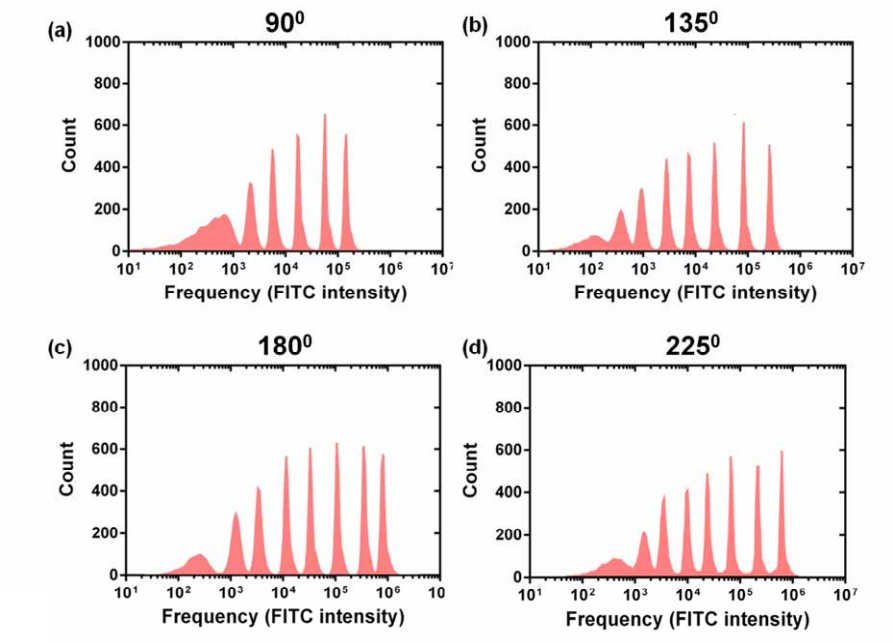

Fig. S3: Comparison of 8 peak rainbow calibration results obtained with 90^0, 135^0, 180^0, and 225^0 microflow cytometry devices. The results show that 1) the 90^0 focusing device cannot distinguish 6^{th}, 7^{th}, and 8^{th} peaks; 2)the 135^0 and 225^0 focusing device can distinguish 8 peaks although the 7^{th} and 8^{th} peak are merged together in both cases; and 3) the 180^0 focusing device evidently shows well distinguished and well separated 8 peaks.

Fluorescence detection of HEK 293 cells:

To characterize the different angled focusing devices, flow cytometric measurements with HEK 293 cells were performed and compared to a commercial flow cytometer (Beckman and Coulter). The cells were stained with Calcein AM (Life Technologies, USA) for detection of fluorescence signals. The laser-induced fluorescence system was used for illuminating 488 nm laser. 525 nm optical filter was used for detection of emission signal. Fig. S4 depicts the results as histogram obtained of fluorescent signals from stained HEK 293 cells detected by 70^0, 90^0, 135^0, 180^0, and 225^0 focusing devices with CV of 25.90%, 21.64%, 17.46%, 13.35%, and 16.23%, respectively. Although all of the devices indicate a single population of cells, the 180^0 focusing device indicates the results that are most comparable (Fig. 8(c)) to commercial flow cytometer (Beckman and Coulter). Notably, the comparison of CVs of the 180^0 focusing device and the commercial flow cytometer (13.35% and 12.87%, respectively) indicates the improvement in the precision of the 180^0 focusing device as compared to other curvature angles.

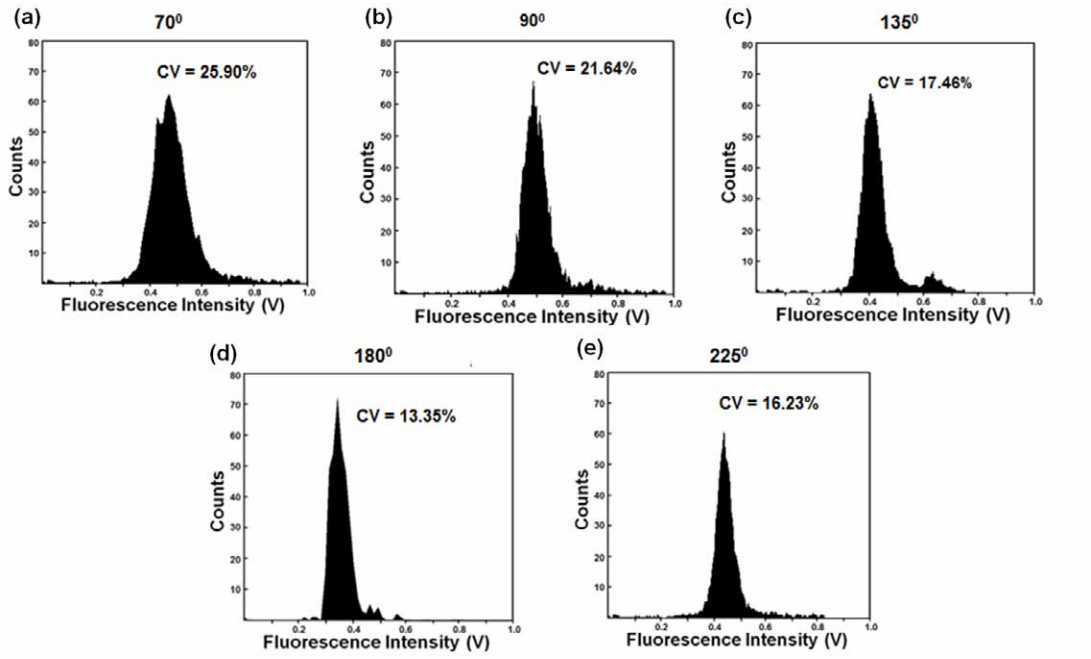

Fig. S4: CV results of HEK 293 cells with 70^0, 90^0, 135^0, 180^0, and 225^0 curvature microfluidic flow cytometry devices

Underlying mechanism of focusing: counter-rotating vortices

The underlying mechanism of microfluidic drifting based 3D focusing is depicted in Fig. S5. The vortices shown at different regions of channel cross-section indicate the fluid behavior. The channel cross-section at A indicates the introduction of sample fluid (red vectors) into the vertical sheath fluid. As the fluid moves around the channel curvature, the centrifugal force causes the sample fluid to bulge away from the inner channel wall into the vertical sheath fluid. This is shown at cross-section B. As the fluids move further around the curvature, the counter-rotating vortices (as a result of centrifugal forces) further stretch the sample fluid towards channel outer wall, as represented by counter-rotating vortices above and below the horizontal middle plane as depicted in cross-section C.

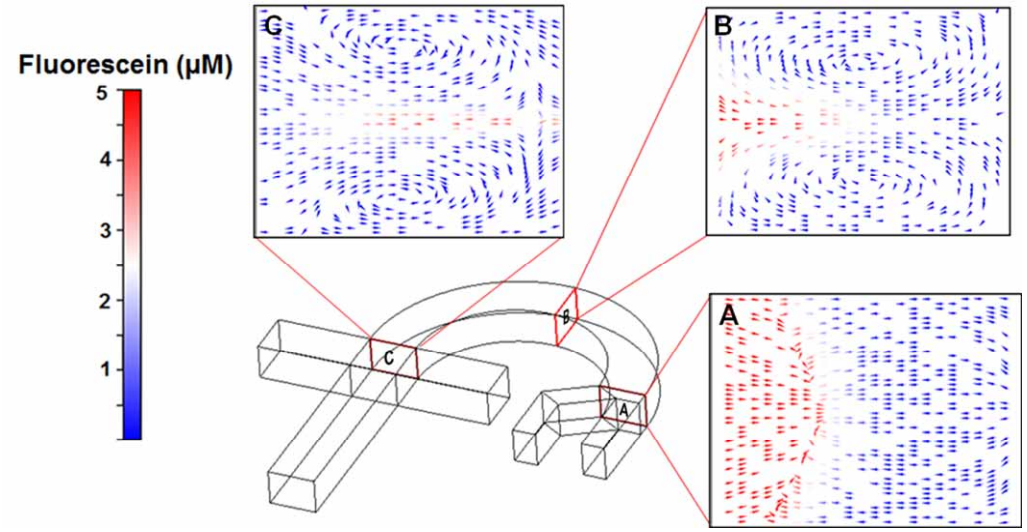

Fig. S5: Counter-rotating vortices above and below the middle plane at the indicated channel cross-sections.

Supporting Videos:

Video S1: The video elucidates 7.32 μm polystyrene beads flowing through a "microfluidic drifting" 3D focusing device with a curvature angle of 135^0. The movie was recorded at 225,000 frames per second. A focusing diameter of ~8.5 μm and a standard deviation of ±0.6 μm in focal position were achieved. Small amounts of food dye were added to the polystyrene bead solution in order to facilitate experimental observation.

Video S2: The video elucidates 1.9 μm polystyrene beads flowing through a "microfluidic drifting" 3D focusing device with a curvature angle of 180^0. The movie was recorded at 225,000 frames per second. A focusing diameter of ~ 2.5 μm and a standard deviation of ±0.45 μm in focal position were achieved. Small amounts of food dye were added to the polystyrene bead solution in order to facilitate experimental observation.

Video S3: The video shows a high concentration ($5x10^6$/ml) of 1.9 μm polystyrene beads flowing through a "microfluidic drifting" 3D focusing device with a curvature angle of 180^0. The video was recorded at 100,000 frames per second. A small amount of food dye was added to polystyrene bead solution to show the beads following the main channel axis. Moreover, the video indicates that the beads remain focused along the main channel axis, even at 1 mm downstream. These results show congruency with the confocal microscopy results shown in Fig. 3. Importantly, it can be noted that before the polystyrene beads flow into the curved channel, they appear unfocused in the Z-plane. However, as the polystyrene beads move around the curve, they are vertically focused in the Z-plane and ultimately confined in three dimensions into a focal diameter of ~ 2.8 μm along the downstream channel.